Modeling and ADRC Control of an Electric Vehicle with a Permanent Magnet Synchronous Machine Fed by an NPC Three-level Inverter

Oumaima Joraiche[1,*], *Abdelmajid* Abouloifa[1], *Elhoussin* Elbouchikhi[2], *Ibtissam* Lachkar[1], *Chaouqi* Aouadi[1], and *Abdelali* El Aroudi[3]

[1]ESE Laboratory, ENSEM, Hassan II University of Casablanca, Casablanca, Morocco
[2]ISEN Yncréa Ouest, Nantes, France
[3]Department d'Enginyeria Electronica, University Rovira i Virgili, Tarragona, Spain

Abstract. The environmental impact of conventional vehicles, mainly due to the air pollutants and greenhouse gas emissions associated with their operation, has accelerated the development of electric transportation. Among the available alternatives, battery electric vehicles (BEVs) have gained considerable attention as a practical approach to reducing emissions from the transport sector. Most electric traction systems use three-phase permanent magnet synchronous machines (PMSMs), mainly because they provide high efficiency, compact size, and accurate torque control. Their performance can be further improved by supplying them through a three-phase, three-level neutral-point-clamped (NPC) inverter. Compared with a conventional two-level inverter, this topology reduces the voltage stress applied to each semiconductor device and produces output voltages with lower harmonic distortion. It can also limit switching losses and improve the quality of the currents supplied to the machine. In this work, Active Disturbance Rejection Control (ADRC) is applied to the current and speed control loops of the traction drive. The closed-loop performance is evaluated in terms of reference tracking accuracy and disturbance rejection capability.

1 Introduction

The growing environmental cost of road transport has pushed the automotive industry to reconsider the widespread use of internal combustion engines. Battery electric vehicles (BEVs) are now being developed as one of the main options for reducing greenhouse gas emissions and air pollution in urban areas. Their effectiveness, however, depends strongly on the traction machine, which must operate efficiently while maintaining good dynamic behavior under changing driving conditions.

The electric machine plays a major role in this system. Permanent-magnet synchronous machines (PMSMs) are widely used in electric vehicles because they combine high efficiency with a compact structure and a high torque density [1]. Their response is also well suited to traction applications when the current and speed loops are properly designed. Still, the behavior of the drive does not depend on the machine alone. The inverter supplying the PMSM

*e-mail: oumaima.joraiche.doc23@ensem.ac.ma

and the selected control method have a direct effect on current quality, torque response, and overall system operation.

In medium- and high-power applications, a three-level neutral-point-clamped (NPC) inverter can be used instead of a conventional two-level topology. The dc-link voltage is shared between several semiconductor devices, which lowers the voltage applied to each switch [2]. The presence of an intermediate voltage level also reduces the size of the voltage steps at the inverter output. This produces waveforms with lower harmonic content and limits the voltage stress applied to the stator windings. Switching losses may also be reduced, depending on the modulation strategy and operating point.

The NPC topology nevertheless makes the control task more demanding. The drive must keep a stable response during acceleration, regenerative braking, speed reversals, and sudden changes in load torque. At the same time, the stator currents must follow their references with limited overshoot and a sufficiently fast settling time. PI controllers are still commonly adopted because they are simple and require little computational effort. Their tuning is usually based on nominal parameters, which means that changes in resistance, inductance, or load conditions can affect the closed-loop response. For this reason, a control method capable of estimating and compensating for such variations is considered in this work.

Active Disturbance Rejection Control (ADRC) offers an alternative approach to this problem. Instead of relying only on a detailed description of the plant, ADRC estimates the combined effect of unmodeled dynamics, parameter variations, and external disturbances through an extended state observer. The estimated disturbance is then compensated within the control law. This principle has motivated the application of ADRC to electrical drives and power conversion systems [3, 4].

Several studies have reported the use of ADRC for the control of power electronic converters. The method has been investigated for dc-link voltage regulation, converter current control, and harmonic reduction under changing operating conditions [5–7]. Linear ADRC and its modified forms have also been applied to bidirectional DC–DC converters, where parameter variations and power-flow reversals can affect the closed-loop response [8]. These results suggest that ADRC may also be suitable for the current and speed control loops of an NPC-fed PMSM traction drive.

In this paper, a three-phase PMSM supplied by a three-level NPC inverter is considered. A mathematical model of the complete traction system is first established, including the vehicle dynamics, the electrical machine, and the power converter. ADRC-based controllers are then developed for the stator current and rotor speed loops. Their ability to track the imposed references and reject load disturbances is examined under steady-state and transient operating conditions. The proposed control structure is evaluated through MATLAB/Simulink simulations.

The rest of the paper is organized as follows. Section II introduces the vehicle dynamic model. Section III presents the PMSM and NPC inverter models and describes the design of the current and speed controllers. The simulation results are analyzed in Section IV. The main conclusions are summarized in Section V.

2 Vehicle Dynamics Modeling

As shown in Fig. 1, the tractive force F_m required to accelerate a vehicle must equal the sum of several resistive forces that oppose motion and the force required for acceleration. These forces include the aerodynamic drag force F_{aero}, which depends on the vehicle shape and speed, the rolling resistance force F_{rr}, which arises from the deformation of the tires in contact with the road surface, the slope resistance force F_{sr}, which represents the gravitational component opposing motion on an inclined road, and the acceleration force F_{acc}, which is responsible for changing the vehicle velocity according to Newton's second law.

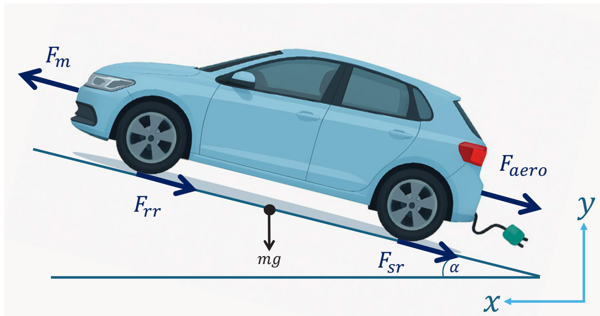

Figure 1: Longitudinal forces acting on the vehicle

Thus, the total force required to propel the vehicle can therefore be expressed as:

$$F_m = F_{\text{aero}} + F_{rr} + F_{sr} + F_{\text{acc}} \tag{1}$$

This equation highlights that the machine must generate sufficient force to overcome aerodynamic drag, rolling resistance, and road-gradient resistance, while also supplying the force needed to accelerate the vehicle to the reference speed. Since the propulsion system generates torque rather than a direct force, this force is converted into a driving torque through the wheel radius and the transmission ratio. The transmission ratio plays a crucial role in adapting the machine rotational speed to the vehicle required speed while ensuring efficient torque delivery [1].

Since the electric motor operates at much higher speeds than the wheels, the transmission system reduces the motor speed while increasing the torque applied to the wheels, ensuring smooth acceleration and sufficient traction. The torque adjustment through the transmission system is expressed as:

$$C_m = \frac{R_{sc}}{R_d} F_m = \frac{C_{m\_wheel}}{R_d} \tag{2}$$

where, C_m represents the driving torque produced by the machine, C_{m_wheel} is the torque applied directly to the wheel, R_{sc} is the tire radius, and R_d is the transmission ratio.

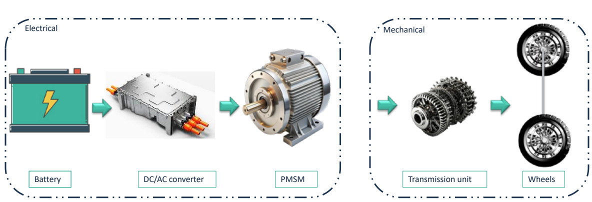

Figure 2: General architecture of an electric vehicle drivetrain.

3 System Modeling and Regulator Design

Speed control of a PMSM is based on cascade feedback control, where the rotor speed is controlled by adjusting the electromagnetic torque. This control is achieved through an outer speed loop, which generates a torque setpoint according to the error between the measured speed and the reference speed, and an inner current loop, which adjusts the stator currents to produce the desired torque. Torque control is achieved by regulating the current i_q in the rotating dq reference frame, while the current i_d is maintained at zero, as shown in Fig. 3.

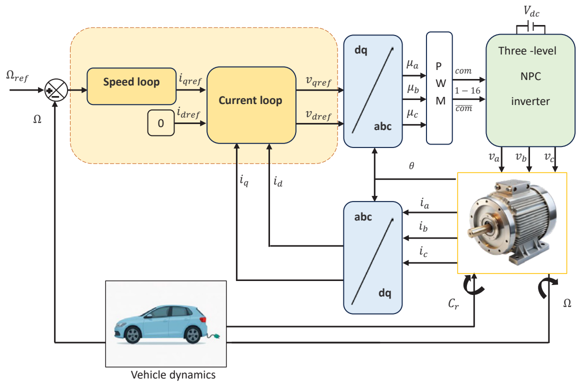

Figure 3: Control structure of the PMSM drive.

3.1 System Modeling

3.1.1 NPC Converter Model

Figure 4 illustrates the power stage of a three-level diode-clamped inverter connected to a PMSM. This multilevel topology uses a split DC bus, where two capacitors divide the DC link into three distinct voltage levels. Each inverter leg comprises four switching devices and two clamping diodes, which limit the voltage stress across each switch to half of the DC-link voltage.

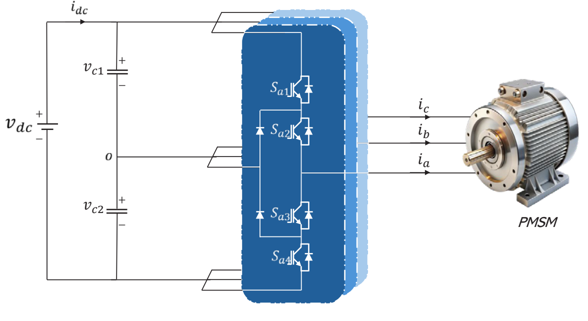

Figure 4: Three-level NPC inverter associated with a PMSM.

The modeling approach begins by formulating the converter equations in the *abc* reference frame, resulting in a static model that describes the instantaneous relationships between the input and output variables:

$$\begin{pmatrix} v_{an} \\ v_{bn} \\ v_{cn} \end{pmatrix} = \frac{1}{3}\begin{pmatrix} 2 & -1 & -1 \\ -1 & 2 & -1 \\ -1 & -1 & 2 \end{pmatrix}\begin{pmatrix} \mu_a & \mu_a^2 \\ \mu_b & \mu_b^2 \\ \mu_c & \mu_c^2 \end{pmatrix}\begin{pmatrix} v_d \\ v_s \end{pmatrix} \tag{3}$$

where,

$$v_s = \frac{v_{c1} + v_{c2}}{2}, \qquad v_d = \frac{v_{c1} - v_{c2}}{2}, \qquad x = a, b, c$$

The switching function of each phase leg is defined as:

$$\mu_x = \begin{cases} +1 \rightarrow S_{x1}, S_{x2} \text{ are ON} \Rightarrow v_{xn} = \dfrac{v_{dc}}{2}, \\ \;\;0 \rightarrow S_{x2}, S_{x3} \text{ are ON} \Rightarrow v_{xn} = 0, \\ -1 \rightarrow S_{x3}, S_{x4} \text{ are ON} \Rightarrow v_{xn} = -\dfrac{v_{dc}}{2}. \end{cases}$$

3.1.2 PMSM Model

The model of the PMSM in the *abc* reference frame is expressed as:

$$\begin{pmatrix} v_a \\ v_b \\ v_c \end{pmatrix} = R_s \begin{pmatrix} i_a \\ i_b \\ i_c \end{pmatrix} + \frac{d}{dt}\begin{pmatrix} \varphi_a \\ \varphi_b \\ \varphi_c \end{pmatrix} \tag{4}$$

where, R_s denotes the stator resistance, $[v_a\ v_b\ v_c]^T$ is the phase voltage vector, $[i_a\ i_b\ i_c]^T$ is the phase current vector, and $[\varphi_a\ \varphi_b\ \varphi_c]^T$ is the magnetic flux vector.

The total flux linkage of each phase is defined as:

$$\begin{pmatrix} \varphi_a \\ \varphi_b \\ \varphi_c \end{pmatrix} = \begin{pmatrix} L_{aa} & L_{ab} & L_{ac} \\ L_{ba} & L_{bb} & L_{bc} \\ L_{ca} & L_{cb} & L_{cc} \end{pmatrix}\begin{pmatrix} i_a \\ i_b \\ i_c \end{pmatrix} + \begin{pmatrix} \varphi_{am} \\ \varphi_{bm} \\ \varphi_{cm} \end{pmatrix} \tag{5}$$

The flux linkages produced by the rotor permanent magnets are given by:

$$\begin{pmatrix} \varphi_{am} \\ \varphi_{bm} \\ \varphi_{cm} \end{pmatrix} = \begin{pmatrix} \varphi_m \cos(\theta_e) \\ \varphi_m \cos\left(\theta_e - \frac{2\pi}{3}\right) \\ \varphi_m \cos\left(\theta_e + \frac{2\pi}{3}\right) \end{pmatrix} \tag{6}$$

where, $\theta_e = P\theta_m$ is the electrical rotor position, θ_m is the mechanical rotor position, and P is the number of pole pairs.

Considering a non-salient PMSM, where $L_d = L_q = L_s$, and applying Park transformation, the system dynamics in the $dq0$ rotating reference frame are obtained as:

$$L_s \frac{di_d}{dt} = -R_s i_d + P\Omega L_s i_q + v_d u_d + v_s u_d^2 \tag{7a}$$

$$L_s \frac{di_q}{dt} = -R_s i_q - P\Omega\left(L_s i_d + \varphi_m\right) + v_d u_q + v_s u_q^2 \tag{7b}$$

$$J \frac{d\Omega}{dt} = \frac{3}{2} P i_q \varphi_m - C_r - f\Omega \tag{7c}$$

Here, R_s and L_s denote the stator resistance and inductance. The mechanical dynamics are characterized by the total inertia J, the viscous friction coefficient f, the rotor speed Ω, and the resistive torque C_r. In the synchronous dq reference frame, i_d and i_q represent the direct- and quadrature-axis stator currents, while u_d and u_q correspond to the inverter control variables.

Since the considered machine is a surface-mounted PMSM, the electromagnetic torque does not depend on i_d and can be expressed only as a function of i_q and the permanent magnet flux. Consequently, $i_d = 0$ is imposed to keep the stator current in quadrature with the rotor flux and simplify the control structure.

The PMSM dynamic model highlights the existence of coupling between the d- and q-axis components. The current equations (7a) and (7b) show that variations in one axis affect the other through cross-coupling terms. Moreover, the mechanical equation (7c) indicates that the generated electromagnetic torque must compensate the load and friction torques, which directly affects the acceleration and overall dynamic response of the machine.

Therefore, a robust control strategy is required to compensate coupling effects, nonlinearities, external disturbances, and parameter uncertainties. In this context, Active Disturbance Rejection Control is adopted since it estimates the total disturbance in real time and actively compensates it, thereby improving robustness and dynamic performance [9, 10].

3.2 Design of Linear ADRC

Active Disturbance Rejection Control, initially introduced by Han [9], provides a framework to address system nonlinearities, external disturbances, and internal uncertainties through real-time estimation and compensation mechanisms. At the core of ADRC lies the Extended State Observer, which augments the system model by treating unknown dynamics and perturbations as extended states to be actively rejected.

The original ADRC formulation uses nonlinear gains, which makes frequency-domain analysis more complex [11, 12]. To overcome this limitation, a linearized version with tunable observer and controller bandwidths was proposed. Linear ADRC retains the disturbance rejection capability of the original method while simplifying implementation and theoretical analysis [10, 13]. In its linear form, LADRC mainly requires the tuning of the observer bandwidth ω_o and controller bandwidth ω_c.

The dynamic model of the PMSM can be reformulated by considering averaged quantities over a switching period. Therefore, (7) becomes:

$$L_s \frac{d\bar{i}_d}{dt} = -R_s \bar{i}_d + P\bar{\Omega} L_s \bar{i}_q + v_d u_d \tag{8a}$$

$$L_s \frac{d\bar{i}_q}{dt} = -R_s \bar{i}_q - P\bar{\Omega}\left(L_s \bar{i}_d + \varphi_m\right) + v_d u_q \tag{8b}$$

$$J\frac{d\bar{\Omega}}{dt} = \frac{3}{2} P \bar{i}_q \varphi_m - C_r - f\bar{\Omega} \tag{8c}$$

where, $\bar{i}_d$, $\bar{i}_q$, and $\bar{\Omega}$ denote the averaged values of the d-axis current, q-axis current, and rotor speed, respectively.

3.2.1 Inner Current Loop

For the current loop, the ESO is designed as:

$$\begin{cases} \dot{\hat{\bar{i}}}_{dq} = \hat{f}_k + b u_{dq} - \beta_1 \left(\hat{\bar{i}}_{dq} - \bar{i}_{dq}\right) \\ \dot{\hat{f}}_k = -\beta_2 \left(\hat{\bar{i}}_{dq} - \bar{i}_{dq}\right) \end{cases} \tag{9}$$

where, f_k represents the total disturbance, defined as:

$$f_k = \begin{cases} f_d = -\dfrac{R_s}{L_s}\bar{i}_d + P\bar{\Omega}\bar{i}_q \\ f_q = -\dfrac{R_s}{L_s}\bar{i}_q - P\bar{\Omega}\bar{i}_d - \dfrac{P\bar{\Omega}\varphi_m}{L_s} \end{cases} \tag{10}$$

Here, u_{dq} is the control input and $b = v_d/L_s$ is the input gain. The control law is written as:

$$u_{dq} = \frac{k_p\left(i^*_{dq} - \hat{\bar{i}}_{dq}\right) - \hat{f}_k}{b} \tag{11}$$

where, k_p is the proportional correction gain and i^*_{dq} is the current reference.

According to the bandwidth tuning method, the ESO gains are selected as:

$$\beta_1 = 2\omega_0, \qquad \beta_2 = \omega_0^2 \tag{12}$$

where, ω_0 is the observer bandwidth of the current loop.

3.2.2 Outer Speed Loop

Assuming that the current loops are sufficiently fast, the mechanical dynamics can be written as:

$$\frac{d\bar{\Omega}}{dt} = \frac{\frac{3}{2}P\bar{i}_{qref}\varphi_m - C_r - C_f}{J} \tag{13}$$

By defining:

$$\begin{cases} x_1 = \bar{\Omega} \\ x_2 = f_v \end{cases} \tag{14}$$

the system to be regulated becomes:

$$\begin{cases} \dot{x}_1 = f_v + b_v\bar{i}_{qref} \\ \dot{x}_2 = \dot{f}_v \end{cases} \tag{15}$$

where,

$$b_v = \frac{1.5P\varphi_m}{J} \tag{16}$$

The ESO of the speed loop is then designed as:

$$\begin{cases} \dot{\hat{x}}_1 = \hat{f}_v + b_v\bar{i}_{qref} - \beta_1\left(\hat{\bar{\Omega}} - \bar{\Omega}\right) \\ \dot{\hat{x}}_2 = -\beta_2\left(\hat{\bar{\Omega}} - \bar{\Omega}\right) \end{cases} \tag{17}$$

The speed-loop control law is expressed as:

$$\bar{i}_{qref} = \frac{k_p\left(\Omega^* - \hat{\bar{\Omega}}\right) - \hat{f}_v}{b_v}, \tag{18}$$

where, Ω^* is the speed reference and k_p is the proportional correction gain.

The ESO gains of the speed loop are computed as:

$$\beta_1 = 2\omega_v, \qquad \beta_2 = \omega_v^2 \tag{19}$$

where, ω_v is the speed-loop observer bandwidth. To preserve the cascade structure and ensure proper time-scale separation, $\omega_v < \omega_0$ must be selected.

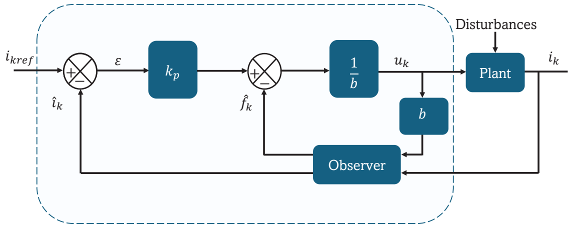

Figure 5: LADRC control schematic diagram.

4 Simulation Results

To evaluate the performance and robustness of the proposed LADRC strategy applied to a PMSM driven by a three-level NPC inverter, detailed time-domain simulations were carried out using MATLAB/Simulink. The vehicle and PMSM parameters used in the simulation are given in Appendix, Tables 1 and 2. The main objective is to assess the controller ability to ensure accurate speed regulation, maintain current tracking performance, and dynamically compensate external disturbances and system uncertainties.

The simulation scenario is designed to expose the system to successive abrupt load variations. A step change in the resistive torque is introduced by modifying the slope angle from 0° to 10° at $t = 0.5$ s, followed by a further increase to 20° at $t = 0.8$ s. The total simulation duration is set to 1 s, allowing a complete evaluation of the dynamic behavior of the drive system.

The current control loops are essential for PMSM operation, since they directly affect torque generation, energy efficiency, and stability. Accurate regulation of the d- and q-axis currents is required to achieve decoupled control between torque and flux components, minimize losses, and improve the dynamic response.

The results shown in Figs. 6a and 6b present the time evolution of the i_d and i_q currents, respectively. As shown in Fig. 6a, the i_d current is regulated around zero despite the applied

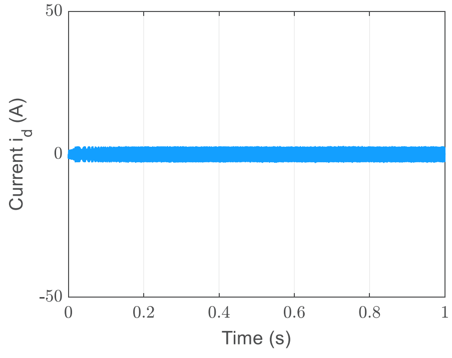

(a) i_d current response.

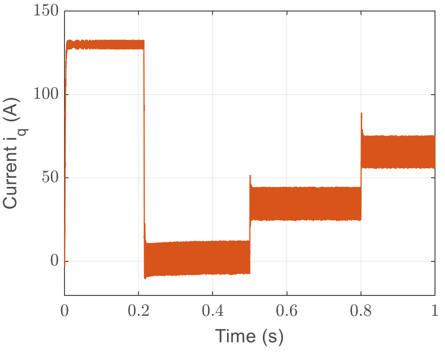

(b) i_q current response.

Figure 6: Current responses.

disturbances, which confirms the effectiveness of the decoupling achieved by the current controller.

Meanwhile, Fig. 6b shows the dynamic adjustment of the i_q current, which represents the torque-producing component. The i_q current increases during acceleration and stabilizes once steady-state operation is reached. When external torque disturbances are applied, the LADRC adjusts the i_q current to provide the additional electromagnetic torque required to compensate the increased load.

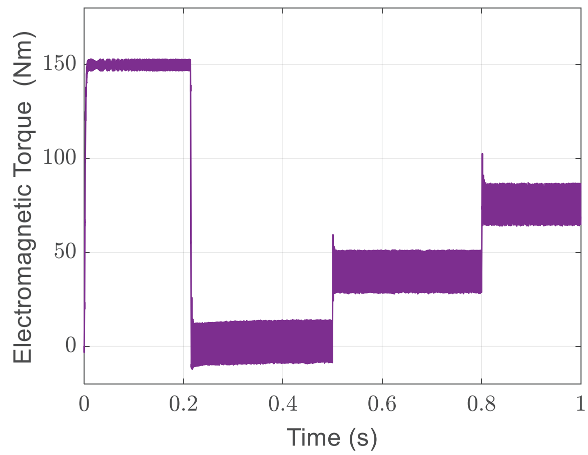

Figure 7: Electromagnetic torque response.

As shown in Fig. 7, the electromagnetic torque exhibits a rapid and stable adjustment, confirming the controller capability to maintain robust performance under time-varying mechanical stress. Regarding the speed response, the rotor mechanical speed closely follows

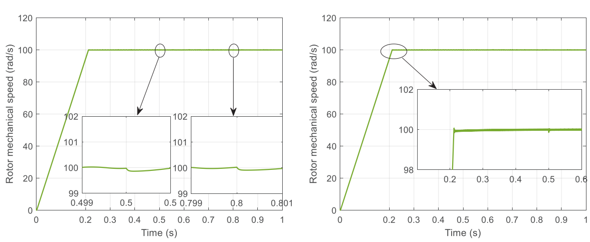

Figure 8: Rotor mechanical speed response.

the reference value of 100 rad/s, with fast convergence and negligible steady-state deviation. When external load disturbances are introduced at $t = 0.5$ s and $t = 0.8$ s, the proposed LADRC maintains consistent speed regulation without significant oscillations or transient instability. Figure 8 highlights the ability of the system to preserve steady-state performance despite abrupt variations in the resistive torque.

5 Conclusion

This paper addressed the modeling and control of a permanent-magnet synchronous machine fed by a three-level neutral-point-clamped inverter. An ADRC scheme was applied to the current and speed loops in order to reduce the effect of load variations and model uncertainties.

The simulation results showed that the controlled drive follows the imposed references with limited tracking error and maintains a stable response when the load torque changes. The obtained results indicate that ADRC is a suitable control option for the studied electric traction system, particularly when disturbance compensation and transient performance are important.

Appendix

Table 1: Vehicle parameters

Parameter	Symbol	Value
Air drag coefficient	C_x	0.302
Rolling resistance coefficient	f_{rr}	0.012
Gravity acceleration	g	$10\,\mathrm{m/s^2}$
Wheel inertia	J_r	$0.75\,\mathrm{kg\cdot m^2}$
Vehicle mass	M	$1500\,\mathrm{kg}$
Wheel radius	R_{sc}	$0.35\,\mathrm{m}$
Equivalent inertia at motor shaft	J_v	$\dfrac{4J_r + MR_{sc}^2}{R_d^2}$
Frontal area	S_f	$2.4\,\mathrm{m^2}$

Table 2: Parameters of the PMSM

Parameter	Symbol	Value
Stator resistance	R_s	$0.05\,\Omega$
Stator inductance	L_s	$0.635\times10^{-3}\,\mathrm{H}$
Rotor inertia	J_m	$11\times10^{-3}\,\mathrm{kg\cdot m^2}$
Viscous friction coefficient	f_v	$0.001889\,\mathrm{Nms/rad}$
Pole pairs number	P	4
Maximum flux linkage	$\varphi_{\max}$	$0.192\,\mathrm{Wb}$
Total inertia	$J = J_m + J_v$	186.7610

References

1. Joraiche, O., Abouloifa, A., Elbouchikhi, E., Lachkar, I., Aouadi, C., Aroudi, A.E.: Performance comparison of PID, ADRC, and backstepping controllers for PMSM speed regulation in electric vehicles. In: 2025 International Conference on Control, Automation and Diagnosis (ICCAD), pp. 1–6 (2025). https://doi.org/10.1109/ICCAD64771.2025.11099472

2. Si, Y., Wang, R., Zhang, S., Zhou, W., Lin, A., Wang, Y.: Fault diagnosis based on attention collaborative LSTM networks for NPC three-level inverters. IEEE Transactions on Instrumentation and Measurement **71**, 1–16 (2022). https://doi.org/10.1109/TIM.2022.3169545
3. Zhou, X., Xu, Q.: Improved active disturbance rejection control for PMSM based on modified extended state observer. In: 2022 4th International Conference on Smart Power & Internet Energy Systems (SPIES), pp. 918–922 (2022). https://doi.org/10.1109/SPIES55999.2022.10082028
4. Xie, X., Zhang, H.: Active disturbance rejection control of permanent magnet synchronous motor based on Kalman filter. In: Proceedings of the 2024 International Conference on Power Electronics and Artificial Intelligence, pp. 929–933 (2024). https://doi.org/10.1145/3674225.3674392
5. Benrabah, A., Xu, D., Gao, Z.: Active disturbance rejection control of LCL-filtered grid-connected inverter using Padé approximation. IEEE Transactions on Industry Applications **54**(6), 6179–6189 (2018). https://doi.org/10.1109/TIA.2018.2855128
6. Zhou, X., Liu, Q., Ma, Y., Xie, B.: DC-link voltage research of photovoltaic grid-connected inverter using improved active disturbance rejection control. IEEE Access **9**, 9884–9894 (2021). https://doi.org/10.1109/ACCESS.2021.3050191
7. Elbouchikhi, E., El Moubarek, A.B., Abouloifa, A., El Aroudi, A., Benbouzid, M.: Active disturbance rejection control for four-wire inverters in standalone renewable resources-based microgrid–islanded microgrids ADRC-based control. ISA Transactions **156**, 290–306 (2025). https://doi.org/10.1016/j.isatra.2024.11.006
8. Zhao, M., Liu, J., Li, L.: Simulation of bidirectional DC–DC converter based on improved linear active disturbance rejection control. In: 2024 IEEE China International Youth Conference on Electrical Engineering (CIYCEE), pp. 1–6 (2024). https://doi.org/10.1109/CIYCEE63099.2024.10846803
9. Han, J.: From PID to active disturbance rejection control. IEEE Transactions on Industrial Electronics **56**(3), 900–906 (2009). https://doi.org/10.1109/TIE.2008.2011621
10. Wu, G., Sun, L., Lee, K.Y.: Disturbance rejection control of a fuel cell power plant in a grid-connected system. Control Engineering Practice **60**, 183–192 (2017). https://doi.org/10.1016/j.conengprac.2016.12.010
11. Herbst, G.: Transfer function analysis and implementation of active disturbance rejection control. Control Theory and Technology **19**, 19–34 (2021). https://doi.org/10.1007/s11768-021-00031-5
12. Tian, G., Gao, Z.: Frequency response analysis of active disturbance rejection based control system. In: 2007 IEEE International Conference on Control Applications, pp. 1595–1599 (2007). https://doi.org/10.1109/CCA.2007.4389465
13. Tang, Y., Bai, Y., Huang, C., Du, B.: Linear active disturbance rejection-based load frequency control concerning high penetration of wind energy. Energy Conversion and Management **95**, 259–271 (2015). https://doi.org/10.1016/j.enconman.2015.02.005